Molecular Therapy
Nucleic Acids
Original Article

Extracellular vesicles mediated exocytosis of antisense peptide nucleic acids

Shipra Malik,[1] W. Mark Saltzman,[2] and Raman Bahal[1]

[1]Department of Pharmaceutical Sciences, University of Connecticut, Storrs, CT 06269, USA; [2]Department of Biomedical Engineering, Yale University, New Haven, CT 06510, USA

Peptide nucleic acids (PNAs), a synthetic DNA mimic, have been extensively utilized for antisense- and antigene-based biomedical applications. Significant efforts have been made to increase the cellular uptake of PNAs, but here we examined relatively unexplored aspects of intracellular trafficking and endocytic recycling of PNAs. For proof-of-concept, we used anti-microRNA (miR) PNA targeting miR-155. The sub-cellular localization of PNA was studied via confocal and flow-cytometry-based assays in HeLa cells. A comprehensive characterization of PNA-containing extracellular vesicles revealed spherical morphology, negative surface charge density, and the presence of tetraspanin markers. Most importantly, we investigated rab11a and rab27b GTPases' role in regulating the exocytosis of PNAs. Organelle staining, followed by confocal imaging, showed higher localization of PNA in lysosomes. Gene-expression analysis established the enhanced functional activity of PNA after inhibition of endocytic recycling. Multiple studies report the exocytosis of single-stranded oligonucleotides, short interfering RNAs (siRNAs), and nanocarriers. To our knowledge, this is the first mechanistic study to establish that PNA undergoes endocytic recycling and exocytosis out of tumor cells. The results presented here can serve as a platform to develop and optimize strategies for improving the therapeutic efficacy of PNAs by avoiding the recycling pathways.

INTRODUCTION

Endocytic recycling is a complex and tightly regulated process that is critical to sustain cellular activities including nutrient uptake, signal transduction, and cytokinesis.[1] The cargoes internalized either via clathrin-dependent or -independent endocytosis undergo different intracellular trafficking pathways. Regardless of the uptake mechanism, the first step of intracellular trafficking for any cargo is early endosome formation, where the vesicle undergoes sorting to be trafficked to the plasma membrane, or directed to the endocytic recycling compartment (ERC), or mature into a late endosome, eventually leading to lysosomes for degradation. The ERC is a microtubular organelle distributed in the cytoplasm[2] and is molecularly defined by the presence of rab11 proteins. Rabs are a class of GTP-binding proteins localized at distinct trafficking compartments; they regulate vesicle formation, fusion, and release from the plasma membrane.[3] The majority of cargo in the ERC is recycled back to the plasma membrane via recycling vesicles, however some fraction is directed to the trans-Golgi network (TGN). Further, rab11 is localized both in the ERC and the TGN and plays a prominent role in regulating the transport of vesicles.[4]

The vesicles released from the plasma membrane by exocytosis are known as extracellular vesicles (EVs). The release of EVs was originally identified as a mechanism for genetic exchange between cells.[5,6] EVs are composed of lipids, proteins, and nucleic acids, containing a cargo of mRNAs, noncoding RNAs, growth factors, and angiogenic factors.[7] EVs, secreted by different cell types, are essential for normal physiological processes including development, immunity, cell migration, and neural function, just to name a few. Similarly, tumor-derived EVs (TEVs), which are present in the tumor microenvironment, promote growth, invasion, metastasis, and tumor resistance.[8] Presently EVs are being extensively explored as a delivery platform for gene-therapy-based applications owing to their biocompatibility, *in vivo* stability, ability to permeate blood brain barrier, and ease of customization.[9,10]

Recently, short interfering RNA (siRNA) has gained immense attention as three siRNA-based drugs, Onpattro, Givlaari, and Oxlumo, received US FDA approval for treatment of amyloidosis, porphyria, and hyperoxaluria, respectively.[11–13] The intracellular trafficking of siRNA-based drugs or drug candidates is still an active field of investigation since their activity is limited by entrapment in sub-cellular compartments.[14] The activity of lipid nanoparticle (LNP)-mediated siRNA delivery is limited due to endosomal entrapment with an escape efficiency of only ~1%–2%.[15] Further, 70% of LNP-containing siRNAs undergo exocytosis by multivesicular late endosomes/lysosomes.[16] The recycling of LNP-containing siRNA is regulated by a 13 transmembrane glycoprotein, Niemann Pick type C1 (NPC1), present on the surface of multivesicular late endosomes, and a small molecule (NP3.47)-mediated inhibition of NPC1 improved the silencing efficiency of siRNA by 4-fold.[17] There is also great interest in single-stranded antisense oligonucleotides (SS ASOs) targeting messenger RNAs (mRNAs); Tegsedi, Spinraza, and Milasen, which have been approved by the US FDA for hereditary transthyretin-mediated amyloidosis,[18] spinal muscular atrophy,[19] and

Received 19 March 2021; accepted 27 July 2021;
https://doi.org/10.1016/j.omtn.2021.07.018.

Correspondence: Raman Bahal, Department of Pharmaceutical Sciences, University of Connecticut, Storrs, CT 06269, USA.
E-mail: raman.bahal@uconn.edu

Batten's disease, respectively. As with siRNAs, endosomal entrapment is a major barrier for SS ASOs. A few studies have demonstrated endocytic recycling of ASOs, as well as nanocarriers via fast recycling, lysosomal, or multivesicular-body-mediated pathways.[20,21]

In this study, we investigated the endocytic recycling of a class of SS ASOs known as peptide nucleic acids (PNAs). PNAs are synthetic DNA mimics in which the phosphodiester backbone is replaced by a pseudo-peptide backbone of N-(2-aminoethyl) glycine units and purine or pyrimidine nucleobases are attached via a methyl carbonyl linker.[22] It has been well established that PNAs bind to the genomic DNA or RNA via Watson and Crick complementary base pairing rules with high specificity and binding affinity.[23] Unlike other ASO chemistries, PNAs are resistant to enzymatic degradation and do not require complex chemical modifications. In addition to antisense applications,[24,25] PNAs have been explored for antigene[26–28] and gene editing[29–31] strategies. PNAs have been extensively used for silencing of microRNAs (miRs), particularly for anti-cancer therapies.[32,33] miRs are small non-coding RNAs, about 22–25 nucleotides (nts) in length, and regulate several physiological processes essential for cell survival, proliferation, and differentiation.[34] Hence, targeting miRs that are overexpressed in tumor (oncomiRs) has emerged as an interesting potential anti-cancer therapy.

However, the clinical translation of PNAs has been impeded by their poor cellular uptake due to their neutral backbone. PNA conjugation with cell penetrating peptides,[35,36] PNA-polyarginine conjugates,[26] and synthesis of gamma modified guanidinium PNAs[37] can improve cellular delivery. Recently, we found that nanoparticle-delivered antimiR PNAs can effectively inhibit tumor growth *in vivo*.[38,39] Although delivery strategies have improved the transfection efficiency of PNAs, endosomal entrapment still limits their availability at the target site. Numerous studies have published ways to improve the cellular uptake of PNAs, but not much effort has been made in studying the endocytic trafficking, as well as exocytosis, of PNAs.

Here, we measured the sub-cellular localization and exocytosis of fluorophore-conjugated PNAs. We designed antimiR PNAs to target miR-155 and miR-21, which are upregulated in several lymphomas, leukemias, and breast cancer among others.[40,41] We performed a comprehensive study of the collection, and inclusive physicobiochemical characterizations of PNA containing TEVs from the treated HeLa cells. We confirmed the tetraspanin markers, on the surface of antimiR PNA containing TEVs and established the role of rab11a and rab27b in the endocytic recycling of PNA containing TEVs. Finally, we determined the impact of recycling and exocytosis of PNAs on their antimiR-155 and antimiR-21 activity. To our knowledge, this is the first study that establishes the endocytic fate of PNAs, including exocytosis and intracellular trafficking. This will serve as a platform for developing and optimizing PNA-based mechanistic and therapeutic studies. In-depth mechanistic studies have provided a basis for clinical application of siRNA-based therapy. We believe that our study will lay the foundation for further research with the goal of making PNA therapeutics a reality in the near future.

RESULTS

PNA design and cellular uptake

We investigated the intracellular trafficking and endocytic recycling of PNAs. First, we designed two full-length PNAs complementary to the miR-155 and miR-21. We conjugated three arginine residues on the N terminus and one arginine on the C terminus of PNAs to achieve high cellular transfection efficiency (Figure 1A). Multiple studies have established that arginine-rich peptides improve the intracellular delivery of PNAs.[26,42,43] Only four arginine residues were conjugated as prior studies reported that excess of positive charge increases the toxicity of PNAs.[25,37] We also conjugated a fluorescent dye, 5-carboxytetramethylrhodamine (TAMRA), on the N terminus of PNAs. The PNA was synthesized using Boc chemistry and established protocols of solid support synthesis.[44–46] PNA purification was performed with high-performance liquid chromatography using water and an acetonitrile-based mobile phase. The observed molecular weight of the purified PNA-155 and PNA-21, measured by mass spectrometry, was found to be similar to the calculated weight of the respective PNAs (Table S1).

First, we examined the time-dependent cellular uptake of PNA-155 containing arginine residues in HeLa cells by confocal microscopy and flow cytometry. HeLa cells were expanded in the logarithmic phase and incubated with the indicated concentrations of PNA-155 followed by confocal microscopy analysis. We observed PNA-155 accumulation inside the cells (Figure S1A) starting from 0.5 h, which increased successively with the duration of incubation. Next, we quantified the cellular uptake at different time points by flow cytometry and noted a higher accumulation of PNA in the cells with increasing incubation time (Figure S1B).

To determine the role of endocytosis in the PNA-155 cellular uptake, we performed temperature-dependent (4°C versus 37°C) cellular uptake studies. We noted that the uptake of PNA-155 decreased significantly in HeLa after incubation at 4°C (Figure S2A). Flow cytometry analysis also showed a 50% decrease in cellular uptake of PNA-155 at 4°C in comparison to 37°C (Figure S2B), suggesting endocytosis as the primary uptake mechanism. PNA-peptide conjugates with cationic residues[43,47] and arginine-rich cell-penetrating peptides have been reported to undergo uptake via endocytosis.[35] However, a few studies have also highlighted the role of non-endocytic routes in facilitating the higher transfection efficiency of arginine-rich peptides.[48] Hence, so far, both endocytic and non-endocytic pathways have been established to contribute to the cellular uptake of arginine residue-containing PNAs.[26,49]

PNA undergoes endocytic recycling

To investigate endocytic recycling, we studied the change in intracellular retention of PNA-155 in HeLa cells by flow cytometry. First, we treated HeLa cells with PNA-155 (4 μM) for 1 h to achieve significant intracellular accumulation. After 1 h, cells were washed and incubated in only media for indicated time points followed by flow cytometry analysis (Figure 1B). The results indicated a significant decrease (~68%) in PNA content after 24 h incubation of treated HeLa cells in fresh medium compared to the PNA content after 1 h (Figures

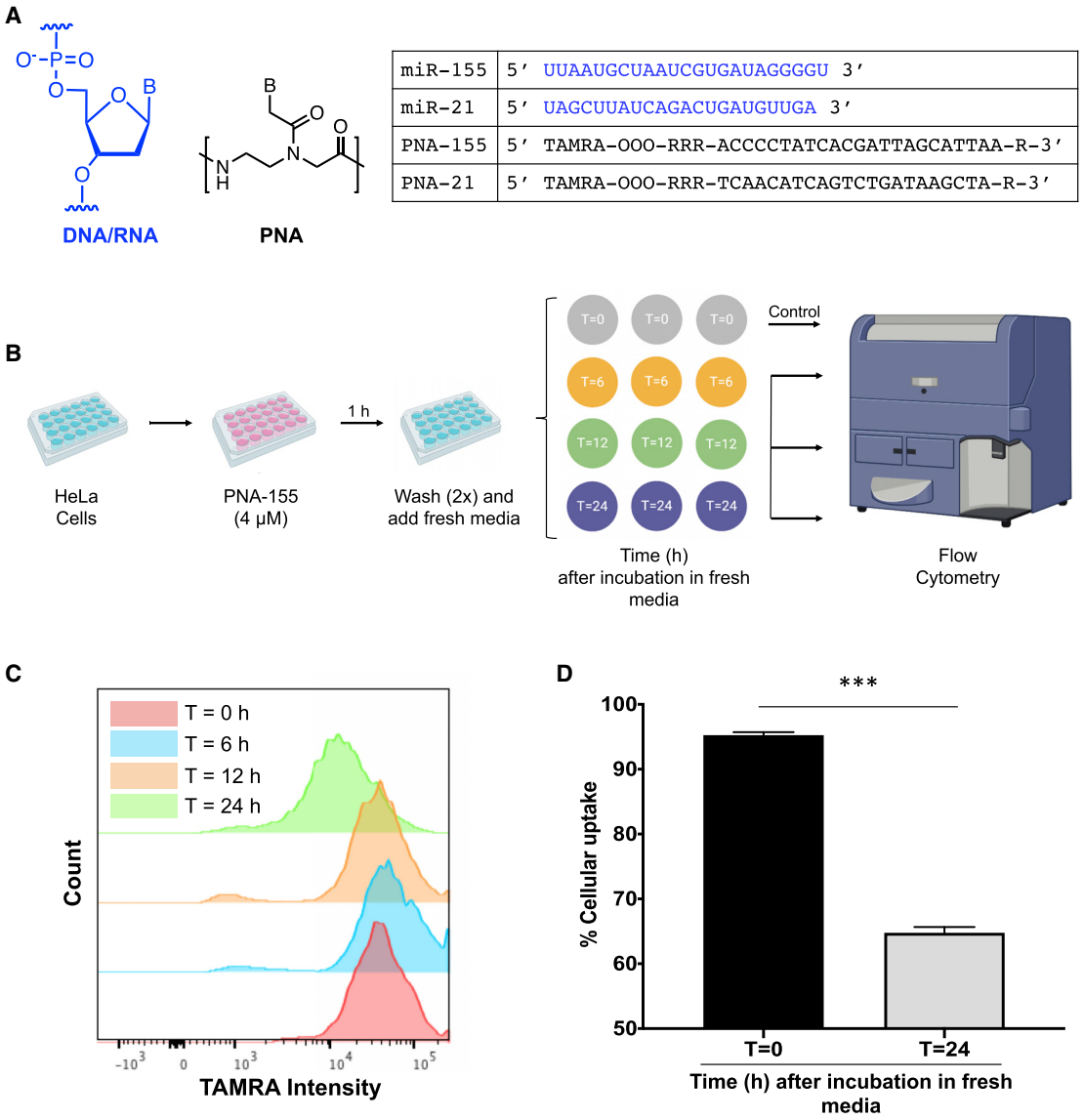

Figure 1. Quantification of exocytosis via flow cytometry

(A) The chemical structure of DNA/RNA and PNA. The table lists the PNA sequences, PNA-155 and PNA-21, complementary to the target miR-155 and miR-21, respectively. (B) Workflow depicting the quantification of exocytosis in HeLa cells using flow cytometry. Samples trypsinized after 1 h treatment with PNA-155 (4 μM) were used as control (T = 0) and treatments were planned accordingly in order to trypsinize all samples at the same time. (C) Representative histogram of exocytosis in HeLa cells at 0, 6, 12, and 24 h of incubation in fresh media followed by quantification of TAMRA intensity in HeLa cells by flow cytometry. 5,000 events were recorded for each sample and all events were included in the histogram. (D) Quantification of HeLa cells with PNA-155 at T = 0 (1 h treatment with PNA-155) and T = 24 h (1 h treatment with PNA-155 followed by washing and 24 h incubation in fresh media). Results are represented as mean ± SEM (n = 3), ***$p < 0.001$.

1C and S3). Since the PNA is stable in cellular extracts,[50] these results suggest that PNA undergoes significant recycling 24 h post-intracellular accumulation in HeLa cells.

Next, we used fluorimetry-based assays to detect the endocytic recycling of PNA-155 in the supernatant medium. Here, we first treated HeLa cells with PNA-155 for 1 h followed by washing and incubation in serum-free medium for indicated time points. We collected the supernatant from incubated HeLa cells and measured the fluorescence at 546 nm/579 nm wavelength (Figure S4A). We observed a gradual increase in fluorescence intensity in the extracellular medium with time, which reached a plateau after 8 h. Further, we exposed the collected supernatant to endosome lysis buffer (1% Triton X-100) and measured the fluorescence at 546 nm/579 nm, which revealed a significant increase (Figure S4B) in fluorescence, indicating that the PNA was trapped inside EVs.

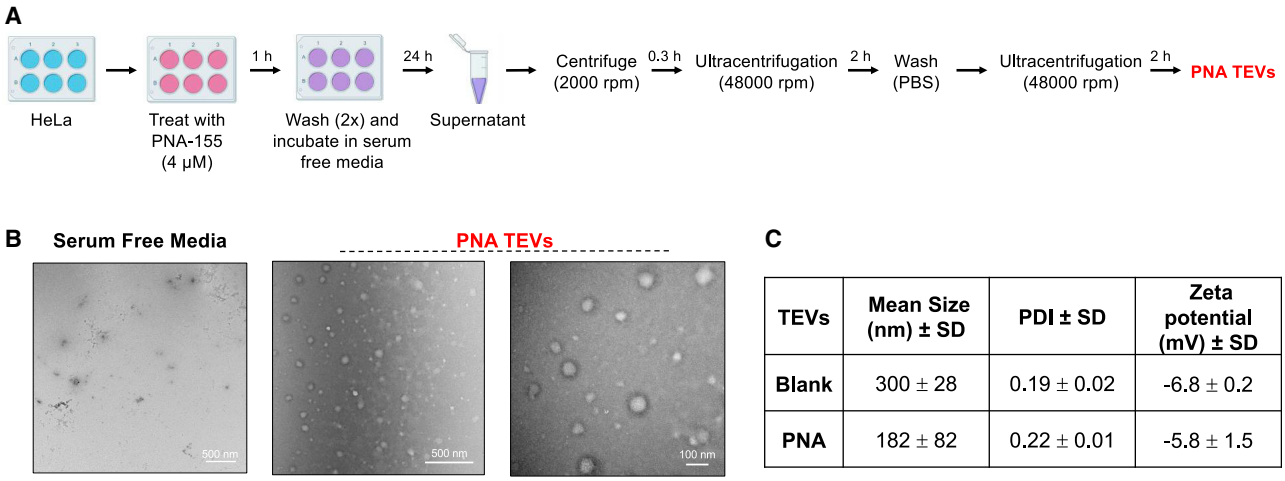

TEVs	Mean Size (nm) ± SD	PDI ± SD	Zeta potential (mV) ± SD
Blank	300 ± 28	0.19 ± 0.02	-6.8 ± 0.2
PNA	182 ± 82	0.22 ± 0.01	-5.8 ± 1.5

Figure 2. Isolation and characterization of tumor-derived extracellular vesicles (TEVs)

(A) Workflow depicting the collection and isolation of TEVs from HeLa cells. HeLa cells treated with PNA-155 (1 h) were washed and incubated in serum-free media for 24 h. Media was collected and ultracentrifuged (2×) to remove supernatant and PNA TEVs were collected. For collection of blank TEVs, serum-free media was collected from untreated HeLa cells and processed via the same procedure. (B) Representative transmission electron microscopy (TEM) images of serum-free media and PNA TEVs. (C) Characterization of TEVs including hydrodynamic diameter, polydispersity index (PDI), and zeta potential. Results were reported as mean ± SD (n = 3).

We also investigated whether the recycling of PNA had an impact on its functional activity. To determine this, we performed RT-PCR to measure the levels of miR-155 in HeLa cells after 1 h treatment with PNA-155 and 24 h washing (Figure S5A). We observed >95% knockdown of the target miR-155 after 1 h incubation with PNA-155. However, 24 h after washing of PNA-155, we noted ~5.5-fold increase (Figure S5B) in the levels of miR-155, indicating that the effectiveness of PNA-155 decreased with time due to the endocytic recycling. We also tested the impact on downstream targets of miR-155 including *FOXO3A* and *BACH1* at 1 h incubation and 24 h after washing.[32] As expected, we noted a ~2-fold decrease in *BACH1* and ~0.5-fold decrease in the levels of *FOXO3A* after 24 h washing of PNA-155 in comparison to the 1 h incubation with PNA-155 (Figures S5C and S5D). Further, we observed an increase in the levels of *BCL-2*, an anti-apoptotic protein, in HeLa cells 24 h after washing of PNA-155 in comparison to the 1 h PNA-155 treated HeLa cells (Figure S5E). Together, these results established that the recycling of PNA-155 in HeLa cells limits its antimiR-155 activity, which further impacts the downstream signaling pathways.

Isolation and characterization of TEVs

To isolate and characterize TEVs, we maintained control (untreated) cells and cells treated with PNA-155 (4 μM) in serum-free medium for 24 h (Figure 2A). We first confirmed the absence of any vesicles in serum-deprived medium by transmission electron microscopy (TEM) analysis (Figure 2B). However, the TEVs isolated from PNA-treated HeLa cells (PNA-TEVs) showed spherical morphology and size range of ~180 nm. The hydrodynamic diameter of TEVs derived from untreated HeLa cells (blank TEVs) when measured via dynamic light scattering was higher (~300 nm) in comparison to the PNA-TEVs (Figure 2C). Further, we noted a similar trend when the size distribution was measured via nanoparticle tracking analysis (NTA; Figure S6). As expected, the surface charge of both blank and PNA TEVs was found to be −6.8 and −5.8 (Figure 2C), respectively, owing to the lipid membranes of EVs.[51]

Treated HeLa-derived TEVs contain PNA and tetraspanin markers

We used flow cytometry to confirm that the TEVs isolated from treated HeLa cells contained PNA. Since TEVs are too small to be detected by flow cytometry directly, we first incubated the TEVs collected from both the untreated and PNA-155 treated HeLa cells with aldehyde beads (3.5 μm) overnight. This allows the TEVs to bind with the surface of aldehyde beads, which can then be analyzed by flow cytometry (Figure 3A). The TEVs derived from treated HeLa cells showed a significant shift toward the TAMRA intensity indicating the presence of PNA within the TEVs. However, TEVs derived from untreated HeLa cells did not demonstrate any shift (Figure 3B).

Next, we investigated the presence of EV markers including tetraspanin CD-63, CD-81, and CD-9 on the surface of TEVs from control and PNA-155-treated cells. Tetraspanin markers are abundantly present in exosomes and other EVs derived from both cancer and non-cancerous cells.[52,53] To quantify the presence of tetraspanin markers on the surface of TEVs, we incubated bead-TEV complexes with fluorescein isothiocyanate (FITC)-conjugated antibodies against CD-63, CD-81, and CD-9 followed by flow cytometry. For blank TEVs, we observed a shift of bead-TEVs complex toward the FITC channel (quadrant 1, Q1) indicating the presence of all three tetraspanin markers (Figure 3C). However, for PNA containing TEVs, we noted the fluorescence shift of bead-TEVs complex to Q2 (upper right), with the TAMRA and FITC channels both indicating the presence of PNA containing TEVs and CD-63, CD-9, and CD-81 tetraspanin markers (Figures 3C and S7). CD-63 showed the

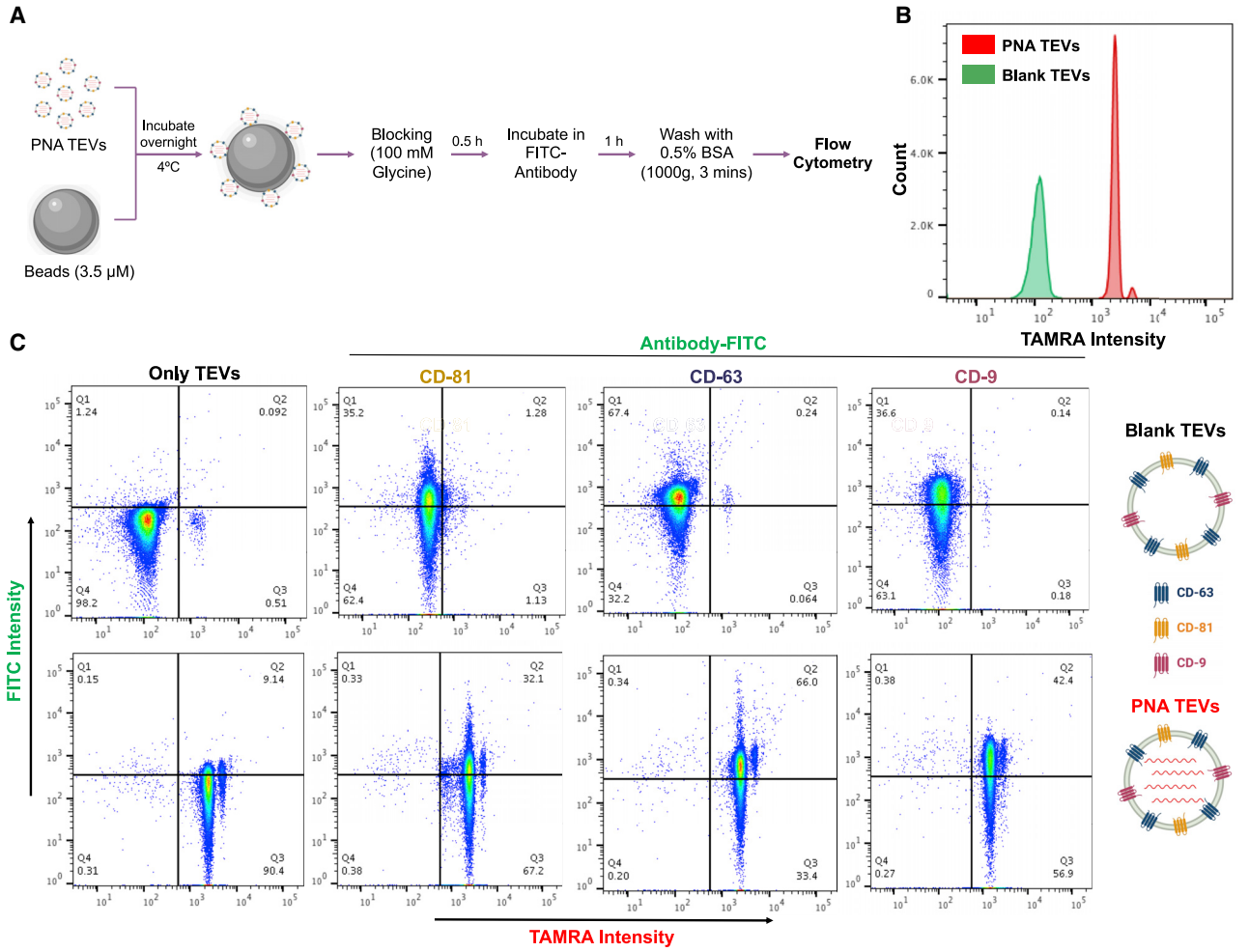

Figure 3. Detection of TEVs via flow cytometry

(A) Workflow depicting the steps used for detection of TEVs using flow cytometry. TEVs were collected from the supernatant of untreated HeLa cells (blank TEVs) or cells treated with PNA-155 (1 h) followed by washing and incubation in serum-free media for 24 h (PNA-TEVs). TEVs collected after ultracentrifugation were conjugated with latex/aldehyde beads followed by incubation of bead-TEVs complex with FITC-conjugated antibodies and detected by flow cytometry. (B) A representative histogram of blank TEVs and PNA TEVs. (C) Representative flow cytometry dot plots of blank TEVs and PNA TEVs showing staining with CD-63, CD-81, and CD-9 FITC-conjugated antibodies. First row represents blank TEVs and second row represents PNA TEVs. The 2nd, 3rd, and 4th columns indicate staining with CD-81, CD-63, and CD-9 antibodies, respectively. 50,000 events were collected for each sample and all events were included in the dot plots.

highest abundance in ~65% PNA-TEVs (Figure S8) followed by CD-9 (~40%) and CD-81 (~30%).

We also incubated the TEVs containing PNA-155 with CD-63 antibody and visualized by confocal microscopy (Figure S9). We noted the presence of PNA-155 within the vesicles and a significant overlap of TAMRA intensity with FITC-conjugated CD-63 antibody. These results further confirmed that PNA is present inside the TEVs with CD-63 as a major marker on surface of TEVs. Further, we used confocal microscopy to investigate whether PNA containing TEVs can undergo cellular uptake when incubated with HeLa cells. We incubated HeLa cells with PNA-155 containing TEVs and observed cellular uptake after 24 h (Figure S10). We observed a prominent intracellular distribution of PNA in cells treated with PNA containing TEVs. These results further corroborated our finding that PNA is present inside the TEVs isolated from treated HeLa cells and can undergo uptake by recipient HeLa cells.

Inhibition of endocytic recycling increases cellular retention and antimiR activity of PNAs

Next, we investigated the role of endocytic recycling pathways on exocytosis of PNAs. Rab11a is a GTPase protein that is localized in the membranes of ERC and TGN,[54,55] whereas rab27b is another protein that belongs to GTPase family and mediates the exocytosis process by regulating the fusion of multivesicular bodies (MVBs) with the plasma membrane.[56] The perturbation of rab11a results in the

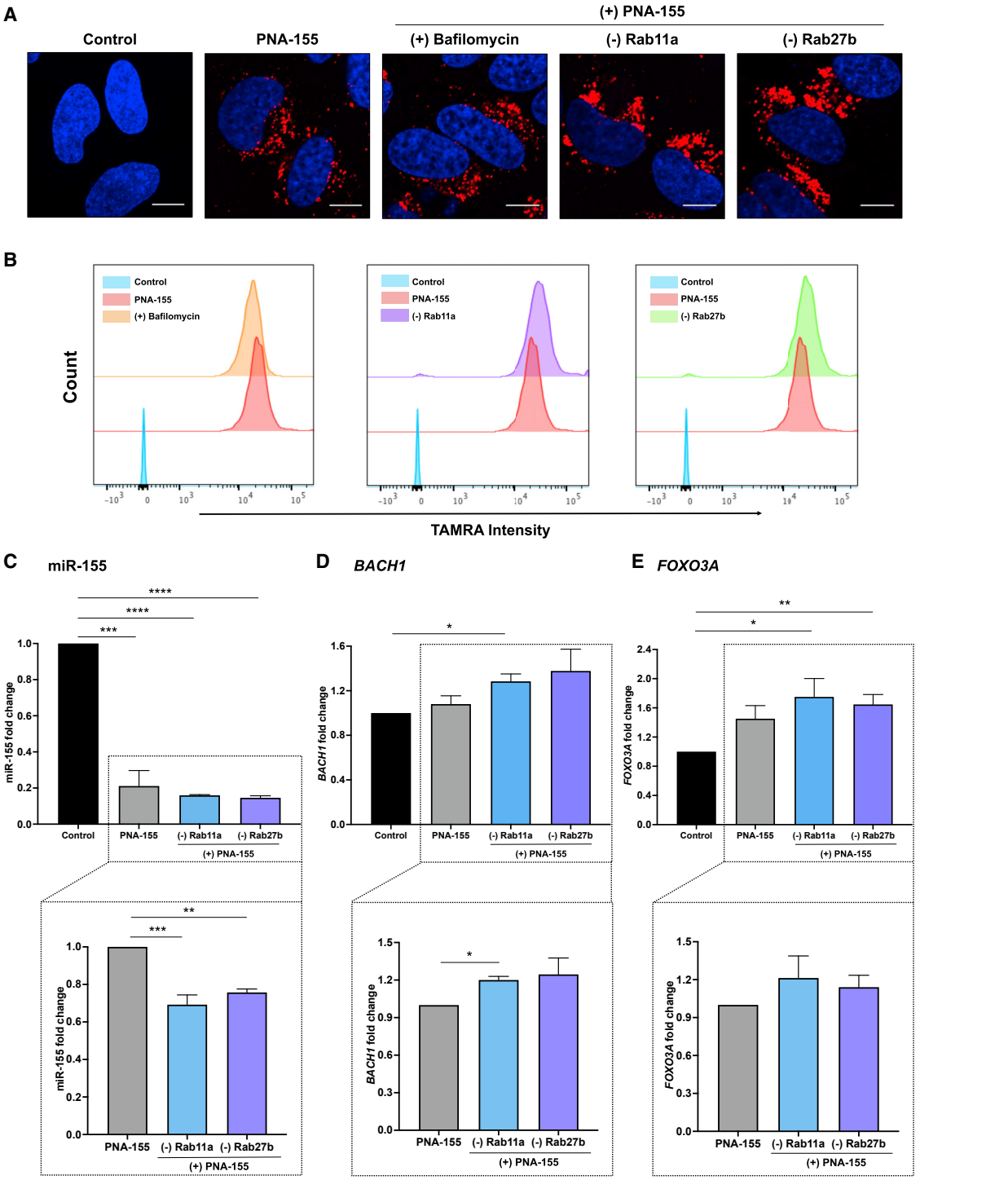

Figure 4. Increased cellular accumulation of PNA after inhibition of endocytic recycling

(A) Fluorescent images of live HeLa cells after 24 h incubation with PNA-155 (4 μM) and inhibition of endocytic recycling using bafilomycin (1 μM), rab11a siRNA (50 nM), and rab27b siRNA (60 nM). HeLa cells were transfected with rab11a and rab27b siRNAs for 12 h and were used for cellular uptake studies. Blue indicates nucleus and red indicates TAMRA. Scale bar represents 10 μm. (B) Cellular uptake of PNA-155 in HeLa cells after 24 h incubation and inhibition of endocytic recycling using bafilomycin, rab11a siRNA, and rab27b siRNA via flow cytometry. 5,000 events were recorded for each sample. (C) The fold change in expression levels of miR-155 in wild-type, rab11a (–), and rab27b (–) HeLa cells after 24 h treatment with PNA-155 in comparison to untreated cells. U6 was used as the reference gene. (D) The fold change in levels of *BACH1*,

(legend continued on next page)

accumulation of transferrin receptors in ERC.[57] The knockdown of rab27b in HeLa cells reduces the time and number of docking events of MVBs with the plasma membrane.[56] Further, rab27b-deficient cells secrete only 50% of vesicles compared to regular cells.[56] Hence, we established cell-based assays in the presence of rab11a and rab27b inhibitors, which regulate distinct steps in the endocytic recycling pathway to gain insight into the intracellular trafficking of PNAs.

First, we optimized the siRNA-mediated knockdown of rab11a and rab27b to achieve optimal endocytic recycling inhibition. We found that rab11a siRNA induced >90% inhibition of the target mRNA at 50 nM dose when measured 72 h post-transfection (Figure S11A). Similarly, ~80% inhibition of rab27b was achieved using 60 nM siRNA at 72 h post-transfection (Figure S11B). Further, we seeded rab11a inhibited (–), rab27b inhibited (–), and un-transfected HeLa cells (wild-type) to study the impact on cellular uptake after 1 h and 24 h of incubation with PNA-155. We also tested the effect of bafilomycin, a vacuolar proton ATPase inhibitor, which prevents the acidification of endosomes, on intracellular trafficking of PNA.[58,59] To study the impact of bafilomycin, we co-incubated HeLa cells with PNA-155 (4 μM) and bafilomycin (1 μM) for 1 h and 24 h.

Confocal microscopy results revealed that inhibition of rab11a and rab27b or use of bafilomycin (1 μM) did not impact the cellular uptake of PNA-155 in HeLa after 1 h of incubation (Figure S12). However, we noted a significantly higher fluorescent signal of PNA-155 in rab11a (–) and rab27b (–) HeLa after 24 h of incubation (Figures 4A and S13A) in comparison to HeLa cells without recycling inhibition. Rab11a (–) and rab27b (–) HeLa cells showed ~2.5 and ~2-fold higher cellular accumulation of PNA-155 (Figures 4B and S13B), respectively, due to the inhibition of endocytic recycling when quantified by flow cytometry. However, we observed a slight decrease in the cellular uptake of PNA-155 when co-incubated with bafilomycin after 24 h. These results were consistent with prior studies with cellular uptake of LNPs in the presence of bafilomycin.[16] We also studied the PNA-155 retention in rab11a (–), rab27b (–), and wild-type HeLa cells after 1 h PNA-155 treatment and 24 h incubation in fresh media via confocal microscopy. We observed higher retention of PNA in both rab11a (–) and rab27b (–) HeLa cells versus wild-type cells indicating that some fraction of PNA does undergo recycling (Figure S14).

We also investigated the impact of rab11a and rab27b siRNA-mediated inhibition of endocytic recycling on antimiR efficacy of both PNA-155 and PNA-21. When compared against the PNA treated wild-type HeLa cells, rab11a (–) HeLa cells showed >30% decrease in levels of miR-155 after 24 h treatment with PNA-155 (Figure 4C). Similarly, rab27b (–) HeLa cells showed ~25% lower miR-155 levels than wild-type cells after 24 h treatment with PNA-155. In addition, we also assessed the levels of *BACH1* and *FOXO3A* in wild-type, rab27b (–), and rab11a (–) HeLa cells after 24 h treatment with PNA-155. The gene expression results showed direct correlation of reduced miR-155 levels with an increase in the downstream targets expression in both rab11a (–) and rab27b (–) HeLa cells. Both PNA-155-treated rab11a (–) and rab27b (–) HeLa cells showed a ~20% increase in the *BACH1* levels in comparison to the PNA-155-treated wild-type HeLa cells (Figure 4D). Similarly, *FOXO3A* levels showed ~20% and 10% elevation in PNA-155-treated rab11a (–) and rab27b (–) HeLa cells, respectively, when compared against PNA-155-treated wild-type cells (Figure 4E). We also tested the antimiR efficacy of PNA-21 by measuring the levels of miR-21 and its direct downstream target, phosphatase and tensin homolog (*PTEN*),[60] in wild-type, rab11a (–), and rab27b (–) HeLa cells after 24 h incubation with PNA-21. We noted a ~35% and ~10% decrease in miR-21 levels in rab11 (–) and rab27b (–) HeLa cells, respectively, in comparison to the wild-type HeLa cells post PNA-21 treatment (Figure S15A). Similarly, as expected, ~20% upregulation in the *PTEN* level was observed in both rab11a (–) and rab27b (–) HeLa cells in comparison to the wild-type HeLa cells (Figure S15B). These results established that inhibition of PNA recycling not only results in higher cellular accumulation but also results in improved functional efficacy of PNAs.

Inhibition of endocytic recycling results in lysosomal accumulation of PNAs

Further, we examined the sub-cellular localization of retained PNA in HeLa cells. We studied the PNA-155 localization in lysosomes, ERC, and in MVBs in rab11a (–), rab27b (–), and wild-type HeLa cells after 24 h of treatment. Confocal microscopy indicated that a significant amount of PNA in rab11a (–) and rab27b (–) HeLa cells accumulated in lysosomes (Figures 5, S16, and S19; Videos S1, S2, and S3). One plausible explanation for these observations is that inhibition of PNA recycling from endosomes to the ERC or TGN directs the excess PNA toward the lysosomes.

Next, we stained rab11a, which is chiefly localized in ERC to study PNA accumulation. Interestingly, only PNA-treated wild-type HeLa cells showed higher localization in ERC (Figures 5, S17, and S19). We observed a minimal overlap of PNA with ERC in rab11a (–) and rab27b (–) HeLa cells. Similarly, rab27b staining indicated that a major fraction of internalized PNA after 24 h in wild-type HeLa cells is present inside the MVBs characterized by the presence of rab27b, which guides them to the plasma membrane for extracellular secretion (Figures 5, S18, and S19). However, rab11a (–) and rab27b (–) HeLa cells showed minimal TAMRA fluorescent signal overlap with the rab27b-containing vesicles. The quantification of confocal images indicated ~2.5-fold higher co-localization of PNA-155 with lysosomes in rab27b (–) HeLa when compared against the wild-type (Figure S20A).

downstream target of miR-155, in wild-type, rab11a (–), and rab27b (–) HeLa after 24 h treatment with PNA-155 in comparison to untreated cells. (E) The fold change in *FOXO3A* levels in wild-type, rab11a (–), and rab27b (–) HeLa after 24 h treatment with PNA-155 in comparison to untreated cells. *GAPDH* was used as reference gene for *BACH1* and *FOXO3A* mRNA levels. In the bottom panel, PNA-155-treated wild-type HeLa was used as control to determine the fold change of miR-155, *BACH1*, and *FOXO3A*. Results are represented as mean ± SEM (n = 3), ****$p < 0.0001$, ***$p < 0.001$, **$p < 0.01$, *$p < 0.05$.

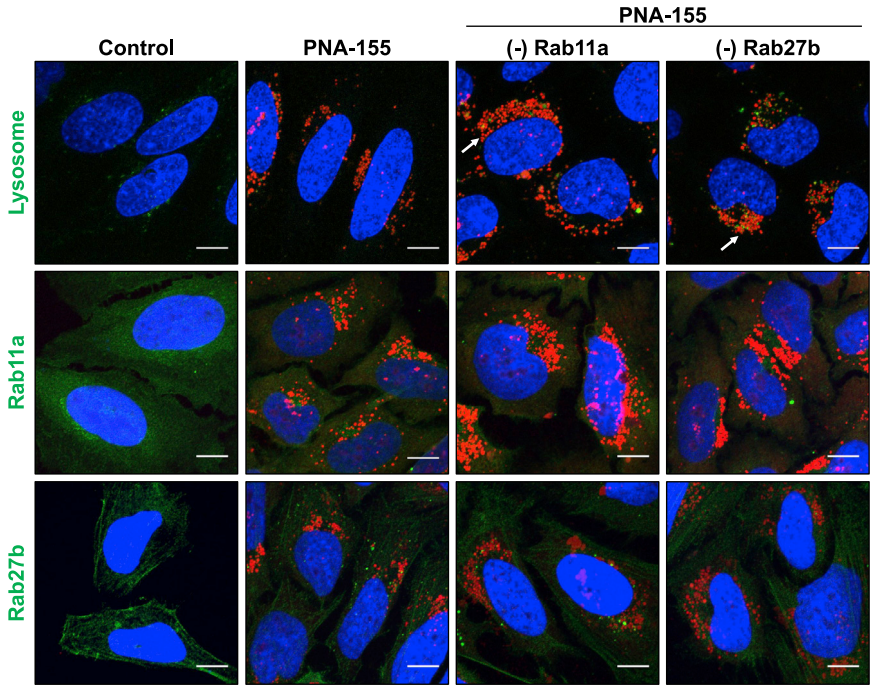

Figure 5. Co-localization study of PNA in lysosomes, ERC (endocytic recycling compartment), and MVBs (multivesicular bodies)

The maximum intensity projection of HeLa cells after 24 h incubation with PNA-155 and inhibition of endocytic recycling using Rab11a siRNA and Rab27b siRNA followed by lysosome (top), rab11a (middle), and rab27b (bottom) staining to determine co-localization. Nucleus was stained using Hoechst dye or DAPI (blue) and red indicates PNA-155. z stacks were recorded with 4 μm step size and maximum intensity projection was obtained using grouped Z projector plugin in ImageJ. The scale bar represents 80 pixels.

Moreover, we noted ~15% and >20% co-localization of PNA-155 with rab11a (ERC) and rab27b (MVBs), respectively, in wild-type HeLa (Figures S20B and S20C). These results indicated that in the absence of recycling inhibition, PNA is significantly associated with the recycling compartment from where it is directed to the plasma membrane for exocytosis.

DISCUSSION

In recent years, significant advances have been made in the field of RNA medicine with the approval and commercial success of several siRNA and SS-ASO-based drugs. Although the clinical utility of RNA therapeutics has been established, the mechanisms of their cellular uptake and intracellular trafficking are not fully understood. Phosphorothioate (PS) RNAs and derivatives have been extensively used in the development of ASO-based drugs. Hence, several studies have investigated the cellular uptake and trafficking of PS-based ASOs to improve their potency and therapeutic index. It has been well-established that the efficacy of PS-ASOs depends on their cellular uptake pathway, which can either enhance their effectiveness or accumulate them in non-productive sinks.[14,61] Similarly, the activity of LNP-delivered siRNAs is circumscribed by endosomal entrapment and recycling.[16] Here, we report the endocytic recycling of another important class of nucleic acid analogs: PNAs. Efforts have been made to improve the cellular uptake of PNAs and study their mechanism of cellular uptake; however, exocytosis or recycling of PNAs during intracellular trafficking has not been previously described. In this study, we isolated and characterized HeLa cell-derived EVs that contain fluorescent-tagged PNA. This study's findings provide a mechanistic understanding of intracellular trafficking of PNAs that can be applied for optimizing its development for clinical applications.

To accomplish this, we designed two PNA sequences targeting miR-155 and miR-21 and conjugated them with four arginine residues to achieve superior transfection efficiency. Prior studies have shown that conjugation of cationic amino acids increases the cellular uptake of PNAs.[62] As expected, our confocal and flow cytometry results showed a time-dependent increase in cellular uptake of PNA-155 in HeLa cells. We observed a significant accumulation of PNA-155 in HeLa cells after 1 h of incubation in growth medium. However, we noticed that the cellular uptake was significantly reduced at low temperatures, indicating the role of endocytosis in the cellular uptake of cationic PNAs. Since cargo that undergoes cellular uptake via endocytosis can be redirected back to the plasma membrane via recycling pathways,[55] we attempted to understand PNA's cellular retention with time after pre-treatment. Our initial flow-cytometry-based quantitative assessment indicated a ~30% decrease in PNA-155 uptake in treated HeLa cells from 1 h pre-treatment to 24 h. This reduction in PNA fluorescent signal indicated the recycling of PNA in HeLa cells.

Gene expression analysis confirmed the impact of PNA recycling on its antimiR efficacy. The miR-155 level increased significantly after 24 h of incubation compared to HeLa cells incubated with PNA-155 for 1 h. Also, direct downstream targets of miR-155, *FOXO3A* and *BACH1*, which are negatively regulated, showed a decrease in their gene expression levels, confirming our results. In addition to low cellular uptake, the entrapment in endosomal/lysosomal compartments limits the availability of PNAs at the target site and is considered a significant hurdle toward its clinical applications. Several strategies, conjugation with cell-penetrating peptides, cyclic peptides, guanidinium PNAs, and endosomal disrupting agents, have been employed to increase PNA efficacy. In this study, we established that the functional activity of PNAs could also be affected by endocytic recycling.

We investigated the recycling of PNA by collecting and characterizing the vesicles derived from tumor cells. The collected TEVs from

treated HeLa cells were found to be in the range of cancer-derived small EVs (<200 nm).[63] The encapsulation of PNAs within the TEVs was quantified via flow cytometry. Further, a higher percentage of CD-63 tetraspanin marker on PNA containing TEVs indicated an endosomal origin.[64] TEVs are secreted by tumor cells in the extracellular matrix, and their role in promoting tumor progression and metastasis has been well established.[65] Furthermore, TEVs can be taken up by recipient cells via internalization, receptor-ligand interaction, or direct fusion.[66] We also noted the cellular uptake of HeLa cell-derived PNA TEVs in recipient HeLa cells via confocal microscopy. A recent study reported that 4T1-derived antimiR-21 loaded TEVs showed transfection in tumor cells, including 4T1 and other tumor cell lines. The uptake of TEVs was not observed in non-malignant cells like HEK or fibroblast cells.[10]

We noticed that inhibition of endocytic recycling pathways via siRNA-mediated knockdown of rab11a and rab27b resulted in higher accumulation of PNA in HeLa cells after 24 h treatment. The role of both GTPases, rab11a, and rab27b, in endocytic recycling has been confirmed in multiple studies.[56,57] Rab11a, localized majorly on ERC and TGN, directed PNA recycling once it entered the cells via endocytosis. Further, inhibition of rab27b prevented the fusion of MVBs with the plasma membrane leading to higher PNA retention in rab27b (–) HeLa cells. The higher cellular accumulation of PNAs due to endocytic recycling inhibition also improved the antimiR efficacy of both PNA-155 and PNA-21 *in vitro*. Gene expression results indicated that miR-155, as well as miR-21 levels, were further reduced upon siRNA-mediated knockdown of rab11a and rab27b in HeLa cells. Rab11a (–) HeLa cells showed the highest antimiR efficacy due to the inhibition of endocytic recycling and PNA's shuttling to TGN. Hence, the PNA stayed in the endosome stage longer as it bypassed the ERC and moved toward the lysosomal stage resulting in greater chances of endosomal escape.

Confocal microscopy revealed that inhibition of rab11a and rab27b results in localization of PNA inside lysosomes. Immunostaining of ERC via rab11a antibody indicated significant localization of PNA within the ERC in the control HeLa cells; however, rab11a (–) HeLa cells did not show any association with ERC. Similarly, intracellular vesicles in wild-type HeLa cells showed the highest association with rab27b stained vesicles in comparison to rab11a (–) or rab27b (–) HeLa cells. Two intracellular fates of MVBs have been reported including fusion with plasma membrane or trafficking to lysosomes.[67] Hence, inhibiting the fusion with plasma membrane by knocking down rab27b can direct the MVBs to the lysosomal compartment. Similarly, perturbation of ERC and TGN by inhibiting rab11a can redirect the sorting endosomes toward the lysosomal stage. These results establish that interruption of the recycling pathway of PNAs via inhibiting either rab11a or rab27b directed the intracellular trafficking toward lysosomal stage. Interestingly, the entrapment of PS-ASOs in lysosomes has been non-productive and limits their activity.[68,69] In contrast, a recent study reported that LNP-delivered GalNAc-siRNA accumulates in the endo-lysosomal compartment and contributes toward sustained siRNA-mediated knockdown of target mRNA.[70] The study demonstrated that siRNA entrapped in the acidic compartments gradually escapes and loads into the RNA-induced silencing complex (RISC) to achieve target knockdown over a period of 3 weeks. Since PNA is resistant to degradation by nucleases or proteases and exhibits high stability,[50] their localization in lysosomes can also contribute to an extended functional activity.

In summary, we demonstrated that PNA endocytosed in HeLa cells is trafficked to ERC and is recycled back to the plasma membrane via MVBs. Further, rab11a and rab27b have a major role in PNA recycling as their perturbation results in higher cellular accumulation of PNA, which also translates into higher antimiR efficacy. We explored the regular PNAs conjugated with cationic amino acids for the mechanistic understanding of its exocytosis/shuttling pathways in the present study. Next-generation gamma PNAs, diethylene glycol (miniPEG), and cyclopentane-based gamma PNAs have been established to exhibit superior binding affinity and efficacy compared to the regular PNAs due to their pre-organized structure.[71–73] It would be significant to study the intracellular uptake and exocytosis of next-generation gamma PNAs in conjunction with the membrane trafficking genes *ex vivo* and *in vivo* to enhance their retention and efficacy.

It would be noteworthy to study the implications of the present study *in vivo* for PNA-based cancer therapeutics. Changes in the expression levels of membrane trafficking genes have been reported in the *in vivo* tumor. The expression of rab proteins, which act as molecular switches of cellular trafficking pathways, are highly dysregulated in cancer.[74] Rab27b is known to be overexpressed in hepatocellular carcinoma,[75] breast,[76] colorectal,[77] and pancreatic cancer[78] and plays an important role in metastasis, tumor invasiveness, and chemoresistance. Multiple studies reported the PNA-based *in vivo* applications; still, exocytosis of the PNAs in the heterogeneous *in vivo* tumor environment considering the altered expression of membrane trafficking genes need to be investigated to modulate its efficacy. Hence it would be interesting to study the combination therapy of rab27b and PNA-based oncomiR inhibition to prevent tumor growth and invasiveness *in vivo*. Further, multiple pathways can contribute toward PNA recycling driven by TGN- or NPC1-mediated exocytosis, as highlighted in LNP recycling. The *in vivo* anti-cancer efficacy of PNAs-based modalities might also be limited by shuttling into non-productive sink. We note that secreted vesicles containing PNA undergo cellular uptake in cancer cells. This also highlights the possibility of distribution of PNA in solid tumors via transcytosis. Moreover, PNA TEVs can also be engineered as a delivery platform for tumor targeting. Better understanding of uptake and intracellular trafficking of PNAs will provide the opportunity to manipulate the internalization and localization to achieve superior efficacy. In addition, PNA design can also potentially alter the cellular uptake pathway and intracellular localization, which determines the functional activity. Our findings highlight the importance of developing PNA chemistries and delivery strategies to optimize cellular transfection and efficient escape from recycling compartments to achieve high efficacy both *in vitro* and *in vivo*.

MATERIALS AND METHODS

Boc-protected monomers were used for synthesis of PNA and were purchased from ASM Research (Germany). 5-carboxytetramethylrhodamine dye (TAMRA) was purchased from VWR (PA, USA). Boc-MiniPEG-3 and Boc-Arginine were bought from Peptide Internationals (KY, USA). Eagle's minimum essential medium (EMEM) and fetal bovine serum (FBS) were purchased from American Type Culture Collection (ATCC; VA, USA). Trypsin-EDTA (0.25%) and opti-MEM reduced serum medium was obtained from GIBCO (Thermo Fisher Scientific, USA). For confocal microscopy, ProLong diamond antifade mountant with DAPI (4',6-diamidino-2-phenylindole) and Triton X-100 (1%) was purchased from Invitrogen (Thermo Fisher Scientific, USA). Aldehyde/sulfate latex bead (4% w/v, 4 μm), FITC-conjugated CD-81, CD-9, and CD-63 antibodies were also obtained from Invitrogen (Thermo Fisher Scientific, USA). Bafilomycin A1 was purchased from Millipore Sigma (MA, USA). The validated rab11a, rab27b siRNAs, and lipofectamine RNAiMAX transfection reagent were purchased from Thermo Fisher Scientific (USA).

Synthesis of PNA oligomer

PNAs were synthesized using standard Boc-chemistry procedures on 4-methylbenzylhydramine (MBHA) resin as reported previously.[44] Three arginine (RRR) residues were conjugated to the N terminus of PNAs followed by miniPEG linker (OOO) and TAMRA dye. PNAs were cleaved from the resin using a cocktail of trifluoroacetic acid (TFA): m-cresol: trifluoromethane sulfonic acid (TFMSA): thioanisole. PNAs were then precipitated from the cocktail with diethyl ether. RP-HPLC was used for purifying the PNAs and molecular weight of purified PNAs was confirmed using mass spectrometry (MALDI-TOF). The concentration of PNAs was determined via UV-Vis spectroscopy using extinction coefficients calculated by combining the extinction coefficient of individual monomers.

Cell culture

HeLa (ATCC CCL-2) cells were cultured in EMEM medium (ATCC 30-2003) supplemented with 10% FBS without antibiotics.

Cellular uptake via confocal microscopy

The cellular uptake of PNA-155 was studied according to previous protocols.[61] For live cell imaging, HeLa cells were seeded in 8-well chambered coverglass (Nunc, Lab-Tek, #155409) overnight and treated with PNA-155 (4 μM) for 0.5, 1, 2, 4, 6, 8, 12, and 24 h. After the specified time point, cells were washed and the nucleus was stained by incubating cells in Hoechst 33342 dye in the incubator. After 20 min, cells were washed with PBS and kept in media during the imaging. For fixed cell imaging, HeLa cells were seeded in 24 well plates, containing a coverslip of 1 mm thickness overnight at a cell density of 50,000 cells/well. After the treatment, cells were washed with phosphate-buffered saline (PBS) twice, followed by incubation in 4% paraformaldehyde (PFA) for 6–8 min at room temperature (RT). After washing, cells were incubated in 0.1% triton for 6–8 min at RT. The coverslips were mounted using the mounting media containing DAPI (#P36966, Invitrogen) on a glass slide. Samples were allowed to solidify overnight and were imaged on a Nikon A1R confocal microscope. The z stacks were captured with 2–4 μm step size. The captured images were processed in ImageJ software to obtain the maximum intensity projection. The quantification of cellular localization was performed using hybrid cell count application in BZ-X800 image analyzer.

Flow cytometry to quantify exocytosis in HeLa

Flow cytometry was performed to quantify the exocytosis of PNA in HeLa cells. HeLa cells were seeded in 24-well plates at a cell density of 50,000 cells/well overnight. The cells were treated at the concentration of 4 μM. After 1 h, cells were washed with PBS (2×) and incubated again in the fresh media. The cells were trypsinized after 0, 6, 12, and 24 h of incubation in fresh media. The treatment of cells with PNA-155 and incubation in fresh media were planned in a manner that all cells were trypsinized at the same time as 24 h samples. Hence, all samples (0, 6, 12, and 24 h after incubation in fresh media) were trypsinized at the same time. The trypsinized cells were washed with PBS followed by centrifugation at 2,000 rpm at 4°C for 3 min and suspended in PBS. The cells were quantified for retention of PNA-155 on a Fortessa X-20 Cell Analyzer at 0, 6, 12, and 24 h of incubation in only media using untreated cells as control. The data analysis was done using FlowJo v10 software.

Isolation of EVs

HeLa cells were seeded in 6-well plates at the cell density of 6×10^5 cells/well overnight. Three wells were incubated with media containing 4 μM PNA-155 and three wells were incubated only in media for 1 h. After 1 h, cells were washed thoroughly with PBS and all wells were incubated in serum free media (without FBS). Here, we used serum-free medium to prevent the background exosomes present in fetal bovine serum. The serum free media from each well was collected after 24 h and subjected to ultracentrifugation according to the established protocols for isolation of tumor-derived vesicles.[79] The collected serum-free media from each well was centrifuged at 2,000 rpm for 20 mins at 4°C to remove cells, debris, and apoptotic bodies. The supernatant was then ultracentrifuged at 48,000 rpm for 120 mins using Beckman Optima XL-90 (Beckman Coulter, IN, USA) and the pellet was resuspended in 2 mL PBS. The PBS was again ultracentrifuged at 48,000 rpm for 120 mins and vesicles in the pellet were collected for further characterization.

Characterization of TEVs

Size and surface charge

Vesicles isolated from both the untreated HeLa cells (blank TEVs) and cells treated with PNA-155 (PNA TEVs) were diluted further in PBS (10× dilution). The hydrodynamic diameter (z-average) of both the blank and PNA TEVs was measured on a Zetasizer (Malvern Panalytical, USA). Further, the charge on surface of TEVs was also determined by measuring the zeta potential at 10× dilution in PBS at 25°C. NTA was used to measure the size distribution of blank and PNA-TEVs at 10× dilution in PBS and 25°C on a Nanosight NS500.

TEM

To determine the size and morphology, we added 10 μL of TEVs sample on copper grid of 400 mesh on carbon support film and incubated for 5–10 mins. TEVs were then washed with 100 μL of 0.5% uranyl acetate to negatively stain the TEVs. The TEVs were allowed to dry at RT. The sample was then imaged using FEI Tecnai G2 spirit BioTwin at 80 kV voltage. The serum-free EMEM media used for collection of TEVs was also negatively stained and imaged using the same procedure.

Detection of TEVs via flow cytometry

Both blank and PNA-TEVs were detected and further characterized for the presence of tetraspanin markers (CD-63, CD-81, and CD-9) on EVs using flow cytometry according to the previously established protocols with some modifications.[6,80] 200 μL of TEVs suspended in PBS were incubated with 5 μL of aldehyde/sulfate latex beads (4% w/v, 4 μm, #A37304) and kept at RT while shaking at 300 rpm for 20 mins followed by shaking at 4°C overnight. TEV beads were collected by centrifugation at 2,000 × *g* for 3 mins. Beads were then blocked in 100 mM glycine (0.4 mL) at RT while shaking at 300 rpm for 0.5 h. Beads were further washed with 0.5% w/v bovine serum albumin (BSA) and collected by centrifugation at 2,000 × *g* for 3 mins. Each TEV-beads sample was then suspended in 200 μL of 0.5% w/v BSA and was further split into four (50 μL) samples. The samples (50 μL) were then incubated with CD-63-FITC (#MA1-19602), CD-81-FITC (#A15753), and CD-9-FITC (#11-0091-82) antibody at RT for 1 h. TEV beads were then centrifuged (2,000 × *g*, 3 mins) and resuspended in 400 μL of 0.5% w/v BSA followed by analysis on a Fortessa X-20. The data analysis was performed using FlowJo v10 software.

Endocytic recycling inhibition

Rab11a siRNA and rab27b siRNA were used for inhibiting two distinct steps of the endocytic recycling. The impact of endocytic recycling inhibitors on cellular uptake, as well as exocytosis of PNA, was studied using immunofluorescence and flow cytometry as detailed below.

siRNA transfection (Rab11a and Rab27b)

Rab11a (assay ID #1672) and rab27b (assay ID #11696) siRNAs were transfected in HeLa cells via reverse transfection using lipofectamine RNAiMAX transfection reagent (Invitrogen, #13778075) according to the manufacturer's protocol. Rab11a siRNA was used at a concentration of 50 nM and rab27b was used at a concentration of 60 nM. For reverse transfection, lipofectamine and siRNA (rab11a and rab27b) were mixed with 200 μL of opti-MEM medium and incubated at RT for 20 mins. About 400,000 HeLa cells suspended in the media were then added to each well in a 6-well plate. Cells were then allowed to adhere and undergo transfection overnight. The transfected cells were washed with PBS and trypsinized followed by collection of the cell suspension and measuring the cell count for further experimental procedures.

Flow cytometry

HeLa cells transfected with rab11a or rab27b siRNA and non-transfected HeLa cells were seeded in a 24-well plate overnight. Cells were treated with PNA-155 (4 μM) for 24 h, washed with PBS, and trypsinized to collect the cell pellet. Cells were suspended in 300 μL PBS and PNA intensity within the cells was quantified via flow cytometry. 5,000 events were recorded for each sample.

Immunofluorescence

HeLa cells transfected with rab11a and rab27b siRNAs and wild-type HeLa cells were allowed to seed in 24-well plate at a cell density of 50,000 cells/well. The HeLa cells with rab11a or rab27b inhibition were incubated with PNA-155 (4 μM) for 1 h and 24 h to determine the impact of rab11a and rab27b inhibition on the uptake of PNA. For immunofluorescence staining, cells were fixed using 4% paraformaldehyde. After permeabilization with 0.1% Triton X-100, cells were blocked for 1 h using 5% w/v BSA at RT. After 1 h of blocking followed by washing, cells were incubated with rab11a primary antibody (Invitrogen, #815300) at 4 μg/mL or rab27b primary antibody (Invitrogen, #PA5-8096) at 1:500 dilution in 1% BSA at 4°C and left overnight in the dark. The following day, goat anti-rabbit immunoglobulin G (IgG; H+L) highly cross adsorbed Alexa Fluor 488 (1:600 dilution, 1% BSA) was used as secondary antibody and incubated at RT for 1 h. After thoroughly washing the cells, they were mounted using antifade mounting media with DAPI and allowed to harden overnight. Images were captured using 60× oil lens in Nikon A1R confocal microscope.

Lysosome staining was performed in live cells by incubating the treated HeLa cells (8 well chambered coverglass) with and without endocytic recycling inhibition (rab11a (–) and rab27b (–) HeLa) in serum-free media containing lysotracker green DND-26 (100 nM; Invitrogen, #L7526) for 40 mins at 37°C. Cells were then washed and nucleus was stained using Hoechst 33342 (Invitrogen, #R37605). The images were captured on a Nikon A1R at 60×. Z stacks were taken at a step size of 2–4 μm and maximum intensity projection of z stacks was obtained using grouped Z-projector in ImageJ.

Gene expression

The cell pellets were collected after indicated time points and total RNA was extracted using RNeasy mini kit (QIAGEN). Next, cDNA was synthesized using a high-capacity cDNA reverse transcription kit (Applied Biosystems). U6 was used as reference for miR-155 and miR-21 levels, while GAPDH was used as a reference gene for *BACH1*, *FOXO3A*, *BCL2*, and *PTEN* mRNA levels. Assay-specific RT primers were used for miR-155 (#467534_mat), miR-21 (#000397), and U6 (#001973). Further, cDNA was amplified and detected using universal master mix with UNG, target-specific primers in CFX connect RT-PCR detection system (Bio-Rad) under the conditions specified in the assay.

SUPPLEMENTAL INFORMATION

Supplemental information can be found online at https://doi.org/10.1016/j.omtn.2021.07.018.

ACKNOWLEDGMENTS

We thank Dr. Anisha Gupta (Wesleyan University) for discussion and suggestions. This work was supported by funds from the

University of Connecticut, UCONN start PPOC award, St. Baldrick's Foundation Jack's Pack: We Still Have His Back, a St. Baldrick's Hero Fund, NIH R01 (CA241194) awarded to R.B., and NIH R01 (CA149128) awarded to W.M.S.

AUTHOR CONTRIBUTIONS

S.M., R.B., and W.M.S. designed the research. S.M. performed the research. S.M., R.B., and W.M.S. did data analysis and manuscript writing.

DECLARATION OF INTERESTS

The authors declare no competing interests.

REFERENCES

1. Steinman, R.M., Mellman, I.S., Muller, W.A., and Cohn, Z.A. (1983). Endocytosis and the recycling of plasma membrane. J. Cell Biol. *96*, 1–27.
2. McGraw, T.E., Dunn, K.W., and Maxfield, F.R. (1993). Isolation of a temperature-sensitive variant Chinese hamster ovary cell line with a morphologically altered endocytic recycling compartment. J. Cell. Physiol. *155*, 579–594.
3. Yamashiro, D.J., Tycko, B., Fluss, S.R., and Maxfield, F.R. (1984). Segregation of transferrin to a mildly acidic (pH 6.5) para-Golgi compartment in the recycling pathway. Cell *37*, 789–800.
4. Wilcke, M., Johannes, L., Galli, T., Mayau, V., Goud, B., and Salamero, J. (2000). Rab11 regulates the compartmentalization of early endosomes required for efficient transport from early endosomes to the trans-golgi network. J. Cell Biol. *151*, 1207–1220.
5. Skog, J., Würdinger, T., van Rijn, S., Meijer, D.H., Gainche, L., Sena-Esteves, M., Curry, W.T., Jr., Carter, B.S., Krichevsky, A.M., and Breakefield, X.O. (2008). Glioblastoma microvesicles transport RNA and proteins that promote tumour growth and provide diagnostic biomarkers. Nat. Cell Biol. *10*, 1470–1476.
6. Valadi, H., Ekström, K., Bossios, A., Sjöstrand, M., Lee, J.J., and Lötvall, J.O. (2007). Exosome-mediated transfer of mRNAs and microRNAs is a novel mechanism of genetic exchange between cells. Nat. Cell Biol. *9*, 654–659.
7. Maas, S.L.N., Breakefield, X.O., and Weaver, A.M. (2017). Extracellular Vesicles: Unique Intercellular Delivery Vehicles. Trends Cell Biol. *27*, 172–188.
8. Zomer, A., and van Rheenen, J. (2016). Implications of Extracellular Vesicle Transfer on Cellular Heterogeneity in Cancer: What Are the Potential Clinical Ramifications? Cancer Res. *76*, 2071–2075.
9. Alvarez-Erviti, L., Seow, Y., Yin, H., Betts, C., Lakhal, S., and Wood, M.J. (2011). Delivery of siRNA to the mouse brain by systemic injection of targeted exosomes. Nat. Biotechnol. *29*, 341–345.
10. Bose, R.J.C., Uday Kumar, S., Zeng, Y., Afjei, R., Robinson, E., Lau, K., Bermudez, A., Habte, F., Pitteri, S.J., Sinclair, R., et al. (2018). Tumor Cell-Derived Extracellular Vesicle-Coated Nanocarriers: An Efficient Theranostic Platform for the Cancer-Specific Delivery of Anti-miR-21 and Imaging Agents. ACS Nano *12*, 10817–10832.
11. (2020). Second RNAi drug approved. Nat. Biotechnol. 38, 385.
12. Dhuri, K., Bechtold, C., Quijano, E., Pham, H., Gupta, A., Vikram, A., and Bahal, R. (2020). Antisense Oligonucleotides: An Emerging Area in Drug Discovery and Development. J. Clin. Med. *9*, 2004.
13. Zhang, M.M., Bahal, R., Rasmussen, T.P., Manautou, J.E., and Zhong, X.B. (2021). The growth of siRNA-based therapeutics: Updated clinical studies. Biochem. Pharmacol. *189*, 114432.
14. Crooke, S.T., Wang, S., Vickers, T.A., Shen, W., and Liang, X.H. (2017). Cellular uptake and trafficking of antisense oligonucleotides. Nat. Biotechnol. *35*, 230–237.
15. Gilleron, J., Querbes, W., Zeigerer, A., Borodovsky, A., Marsico, G., Schubert, U., Manygoats, K., Seifert, S., Andree, C., Stöter, M., et al. (2013). Image-based analysis of lipid nanoparticle-mediated siRNA delivery, intracellular trafficking and endosomal escape. Nat. Biotechnol. *31*, 638–646.
16. Sahay, G., Querbes, W., Alabi, C., Eltoukhy, A., Sarkar, S., Zurenko, C., Karagiannis, E., Love, K., Chen, D., Zoncu, R., et al. (2013). Efficiency of siRNA delivery by lipid nanoparticles is limited by endocytic recycling. Nat. Biotechnol. *31*, 653–658.
17. Wang, H., Tam, Y.Y., Chen, S., Zaifman, J., van der Meel, R., Ciufolini, M.A., and Cullis, P.R. (2016). The Niemann-Pick C1 Inhibitor NP3.47 Enhances Gene Silencing Potency of Lipid Nanoparticles Containing siRNA. Mol. Ther. *24*, 2100–2108.
18. Mathew, V., and Wang, A.K. (2019). Inotersen: new promise for the treatment of hereditary transthyretin amyloidosis. Drug Des. Devel. Ther. *13*, 1515–1525.
19. Wurster, C.D., and Ludolph, A.C. (2018). Nusinersen for spinal muscular atrophy. Ther. Adv. Neurol. Disord. *11*, 1756285618754459.
20. Dahiya, U.R., and Ganguli, M. (2019). Exocytosis - a putative road-block in nanoparticle and nanocomplex mediated gene delivery. J. Control. Release *303*, 67–76.
21. Wu, X.A., Choi, C.H., Zhang, C., Hao, L., and Mirkin, C.A. (2014). Intracellular fate of spherical nucleic acid nanoparticle conjugates. J. Am. Chem. Soc. *136*, 7726–7733.
22. Quijano, E., Bahal, R., Ricciardi, A., Saltzman, W.M., and Glazer, P.M. (2017). Therapeutic Peptide Nucleic Acids: Principles, Limitations, and Opportunities. Yale J. Biol. Med. *90*, 583–598.
23. Rasmussen, H., Kastrup, J.S., Nielsen, J.N., Nielsen, J.M., and Nielsen, P.E. (1997). Crystal structure of a peptide nucleic acid (PNA) duplex at 1.7 A resolution. Nat. Struct. Biol. *4*, 98–101.
24. Bahal, R., McNeer, N.A., Ly, D.H., Saltzman, W.M., and Glazer, P.M. (2013). Nanoparticle for delivery of antisense γPNA oligomers targeting CCR5. Artif. DNA PNA XNA *4*, 49–57.
25. Delgado, E., Bahal, R., Yang, J., Lee, J.M., Ly, D.H., and Monga, S.P. (2013). β-Catenin knockdown in liver tumor cells by a cell permeable gamma guanidine-based peptide nucleic acid. Curr. Cancer Drug Targets *13*, 867–878.
26. Hu, J., and Corey, D.R. (2007). Inhibiting gene expression with peptide nucleic acid (PNA)–peptide conjugates that target chromosomal DNA. Biochemistry *46*, 7581–7589.
27. Janowski, B.A., Hu, J., and Corey, D.R. (2006). Silencing gene expression by targeting chromosomal DNA with antigene peptide nucleic acids and duplex RNAs. Nat. Protoc. *1*, 436–443.
28. Janowski, B.A., Kaihatsu, K., Huffman, K.E., Schwartz, J.C., Ram, R., Hardy, D., Mendelson, C.R., and Corey, D.R. (2005). Inhibiting transcription of chromosomal DNA with antigene peptide nucleic acids. Nat. Chem. Biol. *1*, 210–215.
29. Bahal, R., Ali McNeer, N., Quijano, E., Liu, Y., Sulkowski, P., Turchick, A., Lu, Y.C., Bhunia, D.C., Manna, A., Greiner, D.L., et al. (2016). In vivo correction of anaemia in β-thalassemic mice by γPNA-mediated gene editing with nanoparticle delivery. Nat. Commun. *7*, 13304.
30. Bahal, R., Quijano, E., McNeer, N.A., Liu, Y., Bhunia, D.C., Lopez-Giraldez, F., Fields, R.J., Saltzman, W.M., Ly, D.H., and Glazer, P.M. (2014). Single-stranded γPNAs for in vivo site-specific genome editing via Watson-Crick recognition. Curr. Gene Ther. *14*, 331–342.
31. Ricciardi, A.S., Bahal, R., Farrelly, J.S., Quijano, E., Bianchi, A.H., Luks, V.L., Putman, R., López-Giráldez, F., Coşkun, S., Song, E., et al. (2018). In utero nanoparticle delivery for site-specific genome editing. Nat. Commun. *9*, 2481.
32. Cheng, C.J., Bahal, R., Babar, I.A., Pincus, Z., Barrera, F., Liu, C., Svoronos, A., Braddock, D.T., Glazer, P.M., Engelman, D.M., et al. (2015). MicroRNA silencing for cancer therapy targeted to the tumour microenvironment. Nature *518*, 107–110.
33. Gupta, A., Quijano, E., Liu, Y., Bahal, R., Scanlon, S.E., Song, E., Hsieh, W.C., Braddock, D.E., Ly, D.H., Saltzman, W.M., and Glazer, P.M. (2017). Anti-tumor Activity of miniPEG-γ-Modified PNAs to Inhibit MicroRNA-210 for Cancer Therapy. Mol. Ther. Nucleic Acids *9*, 111–119.
34. Slack, F.J. (2013). MicroRNAs regulate expression of oncogenes. Clin. Chem. *59*, 325–326.
35. Shiraishi, T., and Nielsen, P.E. (2011). Peptide nucleic acid (PNA) cell penetrating peptide (CPP) conjugates as carriers for cellular delivery of antisense oligomers. Artif. DNA PNA XNA *2*, 90–99.
36. Turner, J.J., Ivanova, G.D., Verbeure, B., Williams, D., Arzumanov, A.A., Abes, S., Lebleu, B., and Gait, M.J. (2005). Cell-penetrating peptide conjugates of peptide

nucleic acids (PNA) as inhibitors of HIV-1 Tat-dependent trans-activation in cells. Nucleic Acids Res. *33*, 6837–6849.

37. Thomas, S.M., Sahu, B., Rapireddy, S., Bahal, R., Wheeler, S.E., Procopio, E.M., Kim, J., Joyce, S.C., Contrucci, S., Wang, Y., et al. (2013). Antitumor effects of EGFR antisense guanidine-based peptide nucleic acids in cancer models. ACS Chem. Biol. *8*, 345–352.

38. Babar, I.A., Cheng, C.J., Booth, C.J., Liang, X., Weidhaas, J.B., Saltzman, W.M., and Slack, F.J. (2012). Nanoparticle-based therapy in an in vivo microRNA-155 (miR-155)-dependent mouse model of lymphoma. Proc. Natl. Acad. Sci. USA *109*, E1695–E1704.

39. Malik, S., Lim, J., Slack, F.J., Braddock, D.T., and Bahal, R. (2020). Next generation miRNA inhibition using short anti-seed PNAs encapsulated in PLGA nanoparticles. J. Control. Release *327*, 406–419.

40. Feng, Y.H., and Tsao, C.J. (2016). Emerging role of microRNA-21 in cancer. Biomed. Rep. *5*, 395–402.

41. Higgs, G., and Slack, F. (2013). The multiple roles of microRNA-155 in oncogenesis. J. Clin. Bioinforma. *3*, 17.

42. Manicardi, A., Fabbri, E., Tedeschi, T., Sforza, S., Bianchi, N., Brognara, E., Gambari, R., Marchelli, R., and Corradini, R. (2012). Cellular uptakes, biostabilities and anti-miR-210 activities of chiral arginine-PNAs in leukaemic K562 cells. ChemBioChem *13*, 1327–1337.

43. Saleh, A.F., Arzumanov, A., Abes, R., Owen, D., Lebleu, B., and Gait, M.J. (2010). Synthesis and splice-redirecting activity of branched, arginine-rich peptide dendrimer conjugates of peptide nucleic acid oligonucleotides. Bioconjug. Chem. *21*, 1902–1911.

44. Christensen, L., Fitzpatrick, R., Gildea, B., Petersen, K.H., Hansen, H.F., Koch, T., Egholm, M., Buchardt, O., Nielsen, P.E., Coull, J., and Berg, R.H. (1995). Solid-phase synthesis of peptide nucleic acids. J. Pept. Sci. *1*, 175–183.

45. Malik, S., Slack, F.J., and Bahal, R. (2020). Formulation of PLGA nanoparticles containing short cationic peptide nucleic acids. MethodsX *7*, 101115.

46. Manna, A., Rapireddy, S., Bahal, R., and Ly, D.H. (2014). MiniPEG-γPNA. Methods Mol. Biol. *1050*, 1–12.

47. Bendifallah, N., Rasmussen, F.W., Zachar, V., Ebbesen, P., Nielsen, P.E., and Koppelhus, U. (2006). Evaluation of cell-penetrating peptides (CPPs) as vehicles for intracellular delivery of antisense peptide nucleic acid (PNA). Bioconjug. Chem. *17*, 750–758.

48. Hirose, H., Takeuchi, T., Osakada, H., Pujals, S., Katayama, S., Nakase, I., Kobayashi, S., Haraguchi, T., and Futaki, S. (2012). Transient focal membrane deformation induced by arginine-rich peptides leads to their direct penetration into cells. Mol. Ther. *20*, 984–993.

49. Nakase, I., Niwa, M., Takeuchi, T., Sonomura, K., Kawabata, N., Koike, Y., Takehashi, M., Tanaka, S., Ueda, K., Simpson, J.C., et al. (2004). Cellular uptake of arginine-rich peptides: roles for macropinocytosis and actin rearrangement. Mol. Ther. *10*, 1011–1022.

50. Demidov, V.V., Potaman, V.N., Frank-Kamenetskii, M.D., Egholm, M., Buchard, O., Sönnichsen, S.H., and Nielsen, P.E. (1994). Stability of peptide nucleic acids in human serum and cellular extracts. Biochem. Pharmacol. *48*, 1310–1313.

51. Sancho-Albero, M., Navascués, N., Mendoza, G., Sebastián, V., Arruebo, M., Martín-Duque, P., and Santamaría, J. (2019). Exosome origin determines cell targeting and the transfer of therapeutic nanoparticles towards target cells. J. Nanobiotechnology *17*, 16.

52. Mathieu, M., Martin-Jaular, L., Lavieu, G., and Théry, C. (2019). Specificities of secretion and uptake of exosomes and other extracellular vesicles for cell-to-cell communication. Nat. Cell Biol. *21*, 9–17.

53. Zöller, M. (2009). Tetraspanins: push and pull in suppressing and promoting metastasis. Nat. Rev. Cancer *9*, 40–55.

54. Chen, W., Feng, Y., Chen, D., and Wandinger-Ness, A. (1998). Rab11 is required for trans-golgi network-to-plasma membrane transport and a preferential target for GDP dissociation inhibitor. Mol. Biol. Cell *9*, 3241–3257.

55. Maxfield, F.R., and McGraw, T.E. (2004). Endocytic recycling. Nat. Rev. Mol. Cell Biol. *5*, 121–132.

56. Ostrowski, M., Carmo, N.B., Krumeich, S., Fanget, I., Raposo, G., Savina, A., Moita, C.F., Schauer, K., Hume, A.N., Freitas, R.P., et al. (2010). Rab27a and Rab27b control different steps of the exosome secretion pathway. Nat Cell Biol *12*, 19–30.

57. Ren, M., Xu, G., Zeng, J., De Lemos-Chiarandini, C., Adesnik, M., and Sabatini, D.D. (1998). Hydrolysis of GTP on rab11 is required for the direct delivery of transferrin from the pericentriolar recycling compartment to the cell surface but not from sorting endosomes. Proc. Natl. Acad. Sci. USA *95*, 6187–6192.

58. Bayer, N., Schober, D., Prchla, E., Murphy, R.F., Blaas, D., and Fuchs, R. (1998). Effect of bafilomycin A1 and nocodazole on endocytic transport in HeLa cells: implications for viral uncoating and infection. J. Virol. *72*, 9645–9655.

59. Presley, J.F., Mayor, S., McGraw, T.E., Dunn, K.W., and Maxfield, F.R. (1997). Bafilomycin A1 treatment retards transferrin receptor recycling more than bulk membrane recycling. J. Biol. Chem. *272*, 13929–13936.

60. Meng, F., Henson, R., Wehbe-Janek, H., Ghoshal, K., Jacob, S.T., and Patel, T. (2007). MicroRNA-21 regulates expression of the PTEN tumor suppressor gene in human hepatocellular cancer. Gastroenterology *133*, 647–658.

61. Malik, S., and Bahal, R. (2019). Investigation of PLGA nanoparticles in conjunction with nuclear localization sequence for enhanced delivery of antimiR phosphorothioates in cancer cells in vitro. J. Nanobiotechnology *17*, 57.

62. Hnedzko, D., McGee, D.W., Karamitas, Y.A., and Rozners, E. (2017). Sequence-selective recognition of double-stranded RNA and enhanced cellular uptake of cationic nucleobase and backbone-modified peptide nucleic acids. RNA *23*, 58–69.

63. Möller, A., and Lobb, R.J. (2020). The evolving translational potential of small extracellular vesicles in cancer. Nat. Rev. Cancer *20*, 697–709.

64. Kowal, J., Arras, G., Colombo, M., Jouve, M., Morath, J.P., Primdal-Bengtson, B., Dingli, F., Loew, D., Tkach, M., and Théry, C. (2016). Proteomic comparison defines novel markers to characterize heterogeneous populations of extracellular vesicle subtypes. Proc. Natl. Acad. Sci. USA *113*, E968–E977.

65. Wortzel, I., Dror, S., Kenific, C.M., and Lyden, D. (2019). Exosome-Mediated Metastasis: Communication from a Distance. Dev. Cell *49*, 347–360.

66. Ludwig, A.K., and Giebel, B. (2012). Exosomes: small vesicles participating in intercellular communication. Int. J. Biochem. Cell Biol. *44*, 11–15.

67. Buschow, S.I., Nolte-'t Hoen, E.N., van Niel, G., Pols, M.S., ten Broeke, T., Lauwen, M., Ossendorp, F., Melief, C.J., Raposo, G., Wubbolts, R., et al. (2009). MHC II in dendritic cells is targeted to lysosomes or T cell-induced exosomes via distinct multivesicular body pathways. Traffic *10*, 1528–1542.

68. Juliano, R.L., Carver, K., Cao, C., and Ming, X. (2013). Receptors, endocytosis, and trafficking: the biological basis of targeted delivery of antisense and siRNA oligonucleotides. J. Drug Target. *21*, 27–43.

69. Wang, S., Sun, H., Tanowitz, M., Liang, X.H., and Crooke, S.T. (2016). Annexin A2 facilitates endocytic trafficking of antisense oligonucleotides. Nucleic Acids Res. *44*, 7314–7330.

70. Brown, C.R., Gupta, S., Qin, J., Racie, T., He, G., Lentini, S., Malone, R., Yu, M., Matsuda, S., Shulga-Morskaya, S., et al. (2020). Investigating the pharmacodynamic durability of GalNAc-siRNA conjugates. Nucleic Acids Res. *48*, 11827–11844.

71. He, G., Rapireddy, S., Bahal, R., Sahu, B., and Ly, D.H. (2009). Strand invasion of extended, mixed-sequence B-DNA by gammaPNAs. J. Am. Chem. Soc. *131*, 12088–12090.

72. Sahu, B., Sacui, I., Rapireddy, S., Zanotti, K.J., Bahal, R., Armitage, B.A., and Ly, D.H. (2011). Synthesis and characterization of conformationally preorganized, (R)-diethylene glycol-containing γ-peptide nucleic acids with superior hybridization properties and water solubility. J. Org. Chem. *76*, 5614–5627.

73. Zheng, H., Botos, I., Clausse, V., Nikolayevskiy, H., Rastede, E.E., Fouz, M.F., Mazur, S.J., and Appella, D.H. (2021). Conformational constraints of cyclopentane peptide nucleic acids facilitate tunable binding to DNA. Nucleic Acids Res. *49*, 713–725.

74. Tzeng, H.T., and Wang, Y.C. (2016). Rab-mediated vesicle trafficking in cancer. J. Biomed. Sci. *23*, 70.

75. Dong, W.W., Mou, Q., Chen, J., Cui, J.T., Li, W.M., and Xiao, W.H. (2012). Differential expression of Rab27A/B correlates with clinical outcome in hepatocellular carcinoma. World J. Gastroenterol. *18*, 1806–1813.

76. Hendrix, A., Maynard, D., Pauwels, P., Braems, G., Denys, H., Van den Broecke, R., Lambert, J., Van Belle, S., Cocquyt, V., Gespach, C., et al. (2010). Effect of the

secretory small GTPase Rab27B on breast cancer growth, invasion, and metastasis. J. Natl. Cancer Inst. *102*, 866–880.

77. Bao, J., Ni, Y., Qin, H., Xu, L., Ge, Z., Zhan, F., Zhu, H., Zhao, J., Zhou, X., Tang, X., and Tang, L. (2014). Rab27b is a potential predictor for metastasis and prognosis in colorectal cancer. Gastroenterol. Res. Pract. *2014*, 913106.

78. Li, J., Jin, Q., Huang, F., Tang, Z., and Huang, J. (2017). Effects of Rab27A and Rab27B on Invasion, Proliferation, Apoptosis, and Chemoresistance in Human Pancreatic Cancer Cells. Pancreas *46*, 1173–1179.

79. Kanada, M., Bachmann, M.H., Hardy, J.W., Frimannson, D.O., Bronsart, L., Wang, A., Sylvester, M.D., Schmidt, T.L., Kaspar, R.L., Butte, M.J., et al. (2015). Differential fates of biomolecules delivered to target cells via extracellular vesicles. Proc. Natl. Acad. Sci. USA *112*, E1433–E1442.

80. Suárez, H., Gámez-Valero, A., Reyes, R., López-Martín, S., Rodríguez, M.J., Carrascosa, J.L., Cabañas, C., Borràs, F.E., and Yáñez-Mó, M. (2017). A bead-assisted flow cytometry method for the semi-quantitative analysis of Extracellular Vesicles. Sci. Rep. *7*, 11271.